Behavior of Partially Concrete Encased Steel Beams Under Cyclic Loading
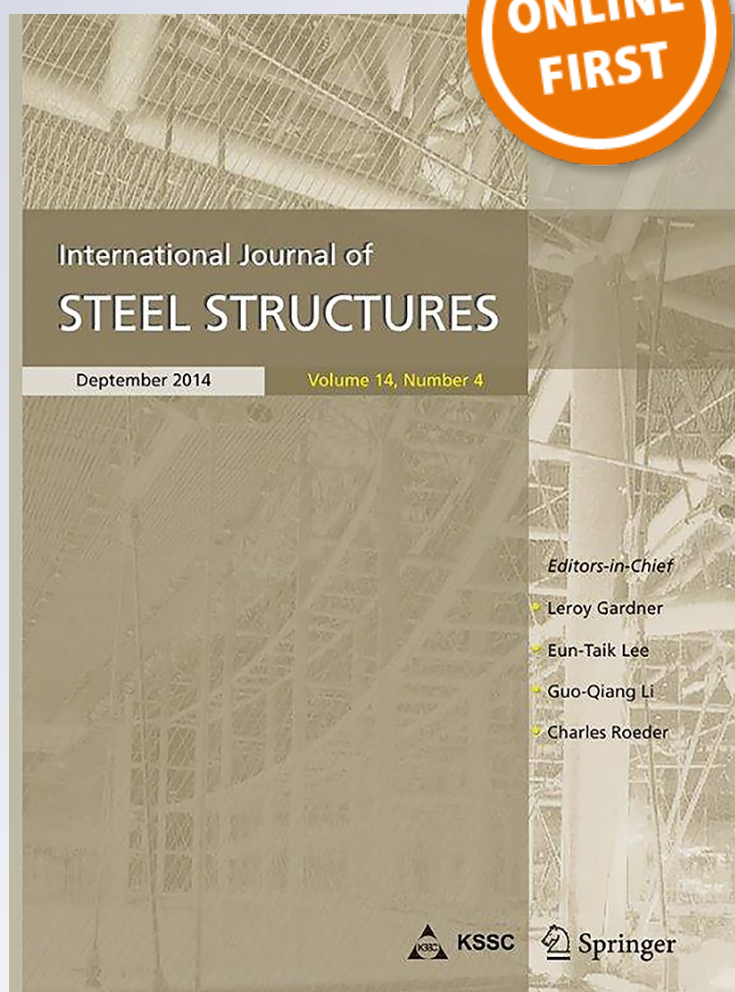
Cheng-Cheng Chen, Teguh Sudibyo & Erwin

ONLINE FIRST

Springer

Springer

CrossMark

Behavior of Partially Concrete Encased Steel Beams Under Cyclic Loading

Cheng-Cheng Chen[1] · Teguh Sudibyo[1,2] · Erwin[1]

Abstract

This paper presents an experimental study of the behavior of partially concrete encased steel beams (PE beams) under seismic loading. The effects of a floor slab in providing lateral and torsional support to the strength and ductility of the beam are also investigated herein. One steel beam and six PE beams were tested herein. The strength development in bare steel beam was insufficient and significant lateral torsional buckling (LTB) was observed. The concrete encasement of the PE beam delayed the occurrence of LTB and hence increased the strength and ductility of the beam. The plastic rotation capacity of PE beam is enhanced by the additional lateral and torsional support provided on the top of a PE beam. For the beam tested in this study, the concrete encasement permits the beam to reach its plastic strength and have plastic rotation of at least 3.42% rad, which is larger than 2% rad required for Intermediate Moment Frames, when no lateral or torsional support is provided at the top of the beam. To satisfy the 4% rad plastic rotation limitation for special moment frames, lateral support with sufficient torsional stiffness is needed.

Keywords Partially concrete encased steel beam · Lateral torsional buckling · Lateral brace · Torsional brace

1 Introduction

Steel beams with top flanges connected to the concrete slab, with or without metal decks, through mechanical anchorage, as shown schematically in Fig. 1, are a common type of building construction. Fire proofing material is usually used to provide fire resistance for the steel members in high-rise buildings. The fire proofing material may cause pollution to the environment; therefore, extra decoration material is often needed to cover the fire proofing material. Fully concrete encased steel beams or steel reinforced concrete (SRC) beams, as shown in Fig. 2a, use concrete to provide fire resistance to the steel in the beam, therefore, the negative effects of fire proofing material can be avoided. However, the concrete brings extra vertical and seismic loads to

the structure; in addition, the construction is comparatively more difficult and requires intensive labor.

The partially concrete encased steel beam, called PE beam hereafter, shown in Fig. 2b, uses concrete in cooperation with fire proofing coating to provide fire resistance. The concrete encasement on PE beam can effectively prevent the temperature of steel from rising sharply in the fire (Kodaira et al. 2004; Piloto et al. 2012, 2013). Compared to SRC beams, this type of beam reduces the amount of concrete used, which reduces the vertical and seismic loads on the structure; in addition, PE beams reduce construction difficulties and cost.

A number of investigation have been carried out to examine the structural performance of PE beams. Kindmann et al. (1993) and De Nardin and El Debs (2009) examined the composite action of PE beams by testing simply supported rectangular beams with monotonic loading. It was proved that the web encasement contributes to the stiffness and flexural capacity significantly, and shear connectors are required for the PE beam to develop a composite action. Nakamura and Narita (2003) presented the use of partially encased composite I-girders as bridge girders, and analytical methods to predict the bending and the shear strength for composite girders were proposed. Hegger and Goralski

✉ Teguh Sudibyo
 d10605809@mail.ntust.edu.tw

[1] Department of Civil and Construction Engineering, National Taiwan University of Science and Technology, No. 43, Keelung Rd, Sec. 4, Da'an Dist., Taipei City 10607, Taiwan (ROC)

[2] Department of Civil Engineering, Universitas Gadjah Mada, Yogyakarta, Indonesia
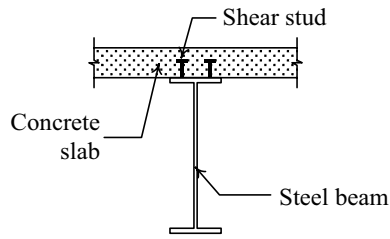
🙅 Springer

Fig. 1 Typical composite flexural member

(2005) evaluated the flexural capacity of PE beams which were integrated with concrete slab under both sagging and hogging moment. The test results showed that, under sagging moment, nearly no difference in the load-deformation behavior between beams with and without shear connection in the encasement. While under hogging moment, the beams without sufficient shear connection showed lower stiffness and flexural capacity. Jiang et al. (2017) investigated the mechanical behavior of the PE beams under hogging moment. It is found that the stiffness and flexural capacity of PE beams increase with the increase in reinforcement ratio of concrete slab. Chen et al. (2017) performed monotonic and cyclic loading test on PE beams with span length of 0.75 m (shear span ratio of 1.5) and 1.5 m (shear span ratio of 3). The test results show that all specimens exceeded the plastic moment capacity and also showed good ductility under both monotonic and cyclic loading.

In the moment resisting frame (MRF), when the beam is subjected to positive moment, which means the top flange is in compression, the concrete slab is considered as having two functions: (1) to work together with steel shape and form a composite section, and (2) to provide lateral support to the top flange of the steel beam to prevent it from lateral-torsional buckling (LTB). However, when the beam is subjected to earthquake type loading, part of the beam is subjected to positive moment and part of the beam is subjected to negative moment. For the beam segment subjected to negative moment, the concrete slab is on the tension side and the composite action is basically negligible. In addition, extra lateral support to the bottom

flange of the steel shape is usually required to prevent the beam from premature LTB. The lateral support provided should satisfy the strength and stiffness requirement for lateral bracing as stated in AISC design code (ANZI/AISC 360-16 2016; ANZI/AISC 341-16 2016). For dwelling buildings, the extra lateral support is often considered as interference with the use of the space in the building. In co-operation with lateral support or lateral support plus torsional bracing provided by the slab, the PE beam, without bottom flange lateral bracing, possibly can be used in earthquake-resistant structures.

At present, research on PE beam focused on the composite action in a PE beam and the design method for a PE beam under monotonic loading and the LTB behavior of the PE beam was not included (Kindmann et al. 1993; De Nardin and El Debs 2009; Nakamura and Narita 2003; Hegger and Goralski 2005; Jiang et al. 2017; Chen et al. 2017). A previous study by Lindner and Budassis (2000) on LTB of PE beams confirmed that PE beams possess higher LTB resistance than bare steel beams. However, the test was conducted under monotonic single curvature loading. The test results from previous research cannot provide a clear understanding regarding the LTB behavior and ductility of a PE beam under seismic loading. In order to assess the applicability of PE beams for earthquake-resistant building structures, the focus here is on the ductility and energy capacity of a PE beam under cyclic type loading.

In steel structures, it is common practice to move the plastic hinge away from the column surface to prevent premature fractures of the welds connecting the beam flange and the column flange. Weakened steel beam-to-column connection have been suggested to solve this problem (Plumier, 1994; Chen et al. 1996; Chen 2001; Itani et al. 2004; Jin and El-Tawil 2005). The weakened beam-to-column connection, also known as a reduced beam section (RBS), is made by trimming off part of the steel flange so the most critical section is not located in the field of welding. Chen et al. (1996) proposed a type of RBS that enlarges the plastic zone and improves the plastic hinge rotation capacity of the beam. In the MRF containing PE

Fig. 2 Concrete encased steel beam **a** Fully concrete encased steel beam/SRC, **b** Partially concrete encased steel beam
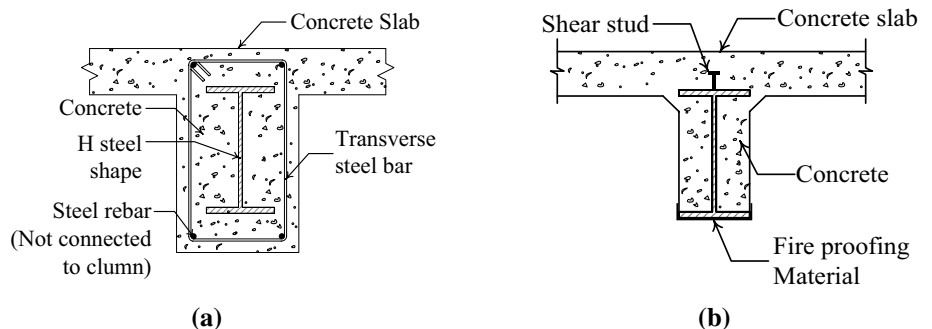
Table 1 Specimen list for H and PE series

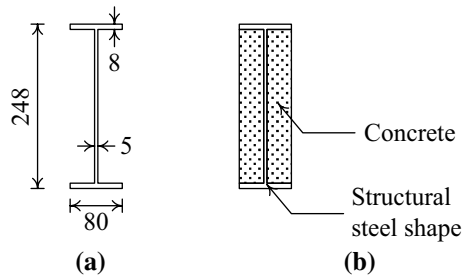| Series	Specimen	Lateral braces	Torsional braces	Shear connectors	Concrete
H	H-0	No	No	No	No
PE	PE-0	No	No	Flange	No
	PE-L	L	No	Flange	No
	PE-LT1	L	T1	Flange	No
	PE-LT2	L	T2	Flange	No
	PEb-LT2	L	T2	Flange	Yes
	PEw-LT2	L	T2	Web	No

Fig. 3 Cross section of beams (unit = mm) **a** H section, **b** PE section

beams, premature fracture of the welds connecting the beam flange and column flange may also occur. And, it is of interest to the authors how PE beams perform when RBS is employed.

An experimental program, utilizing seven beam specimens, was conducted to investigate the behavior of PE beams under cyclic double curvature moment loading. The effects of the concrete encasement, concrete slab and construction details on the behavior of PE beams have been studied herein.

2 Test Specimen and Setup

2.1 Test Specimen

The experimental program includes one H beam specimen, which was designated as H series, and six partially encased H beam specimens, which were specified as PE series, as listed in Table 1. The steel shape used for all the specimens was H248 × 80 × 5×8, as shown in Fig. 3.

Each end of the beam was connected to a column through an end plate connection as shown in Fig. 4. The end plate connection had relatively high strength and stiffness and was considered as rigid connection. The beam length, excluding the thickness of the end plates, was 4400 mm. In order to enhance the ductility of the specimens, RBS (Chen et al. 1996) was used at both beam ends. The geometry of the flange tapering, which was determined based on the steel shape alone, of RBS is shown in Fig. 5. The beam segment CD was selected to yield simultaneously. The plastic moment at D and C was respectively 0.81 and 0.87 M_p, and the projected moment at the beam end was 0.9 M_p, as shown in Fig. 6, where M_p is the nominal plastic moment of the H section.
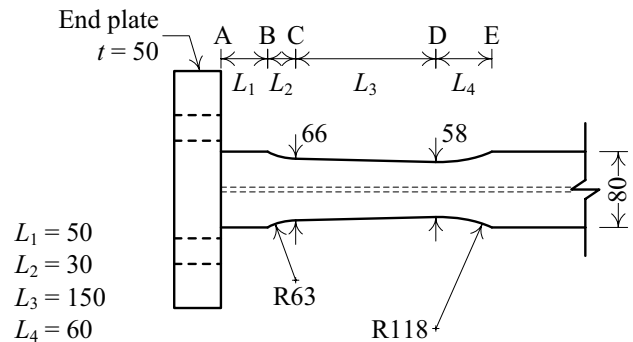

Fig. 5 Detail of flange tapering (unit = mm)

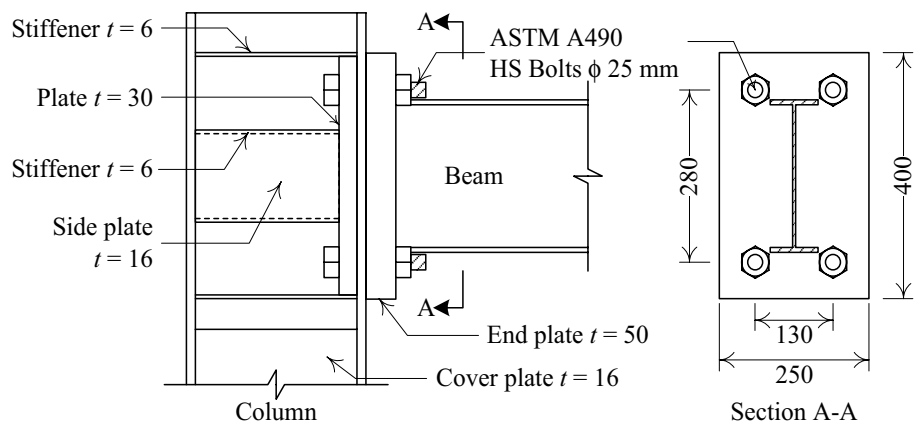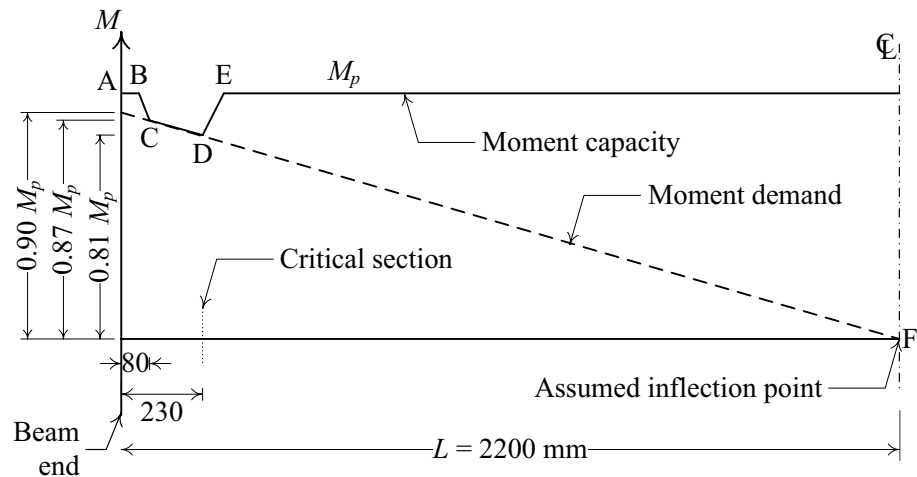**Fig. 4** End plate connection (unit = mm)

Fig. 6 Moment capacity distribution of beam with reduced beam section (RBS)

Various kinds of beam brace configuration were attached to the top flanges of the specimens to take into account the stability effects provided by floor slabs. Specimens with notation "0" had no beam brace attached. Specimens with notation "L" had 11 lateral braces L, with an axial stiffness of 63.8 kN/mm, attached to the top flange as shown in Fig. 7a, b. Specimens with notation "LT1" and "LT2" had 11 lateral braces L and 10 torsional braces T1 or T2 attached at the top flange as shown in Fig. 7a, b. The torsional stiffness of torsional brace T1 and T2 were 4.0 and 16.0 kN-m/radians, respectively. The stiffness of the lateral and torsional braces was calculated based on the nominal size and material properties of the elements. Details of the lateral braces and torsional braces used in this study are shown in Figs. 8 and 9, respectively.

Wire mesh with pitch of wire of 50 mm in both directions was placed in the concrete on both sides of the web for PE specimens, as shown in Fig. 7b–e. All PE specimens, except PEw-LT2, had shear connectors placed on the inner side of the flanges, as shown in Fig. 7b–e, with a spacing of 400 mm. For Specimen PEw-LT2, the shear connectors were connected to the web, as shown in Fig. 7d. All PE specimens, except PEb-LT2, had no concrete in the flange tapering area as shown in Fig. 7c, d. For PEb-LT2, the concrete occupied the space where the flange was tapered, as shown in Fig. 7e.

The steel beams were fabricated through cutting off part of the flanges of hot rolled H248×124×5×8 shapes. The mechanical properties of steel used from material test are shown in Table 2. Due to size limitation of the shear stud available in the market, high strength bolts with a nominal tensile strength of 1220 MPa, as shown in Fig. 7f, were used as shear connectors.

Concrete with maximum aggregate particle size of 10 mm was mixed and cast on one side of the steel beam first. Two days later, the beam was flipped over and the concrete on the other side was cast. Concrete cylinders with diameter

of 10 cm and height of 20 cm were casted and tested. The average compressive strength of the concrete from first and second cast differs less than 5%. Therefore, the average compressive strength of 20.3 MPa was used for beam section moment calculation.

2.2 Test Setup and Instrumentation

As shown in Fig. 10, the test frame is a three-dimensional frame and consists of 4 plane frames, namely S (south), N (north), E (east) and W (west). In the direction of loading, there were Frames S and N, and they were designed in such a way that only Frame S takes the applied lateral load. Frame S, as shown schematically in Fig. 11, contained the test beam, two columns, and a loading beam. Each end of the test beam is connected through the end plate connection, mentioned in the previous section, to the column. The column is H section strengthened by side plates to achieve a relatively much larger moment of inertia compare to that of the test beam. The bottom end of the column is connected through a pin connection to a base beam which is tightened firmly to the strong floor. In order to reduce the axial load that may be induced in the test beam by the applied lateral load, a loading beam with both ends pin connected to the top of the column is used. Ideally, the applied lateral load is then transferred evenly to the top of the columns and results in the moment distribution pattern as shown in Fig. 11.

There were a beam and two columns in frame N and the beam was connected to the columns by pin connections. The bottom end of the column was connected through a pin connection to a steel base tied down to the strong floor. Frames E and W were braced frames which provided stability to the test frame. In addition, a horizontal X-brace was provided just below beam level.

Two linear variable differential transformer (LVDT), LVDT-L and LVDT-R, were attached on frame S at height of H_c measured from center of hinge at column base, as
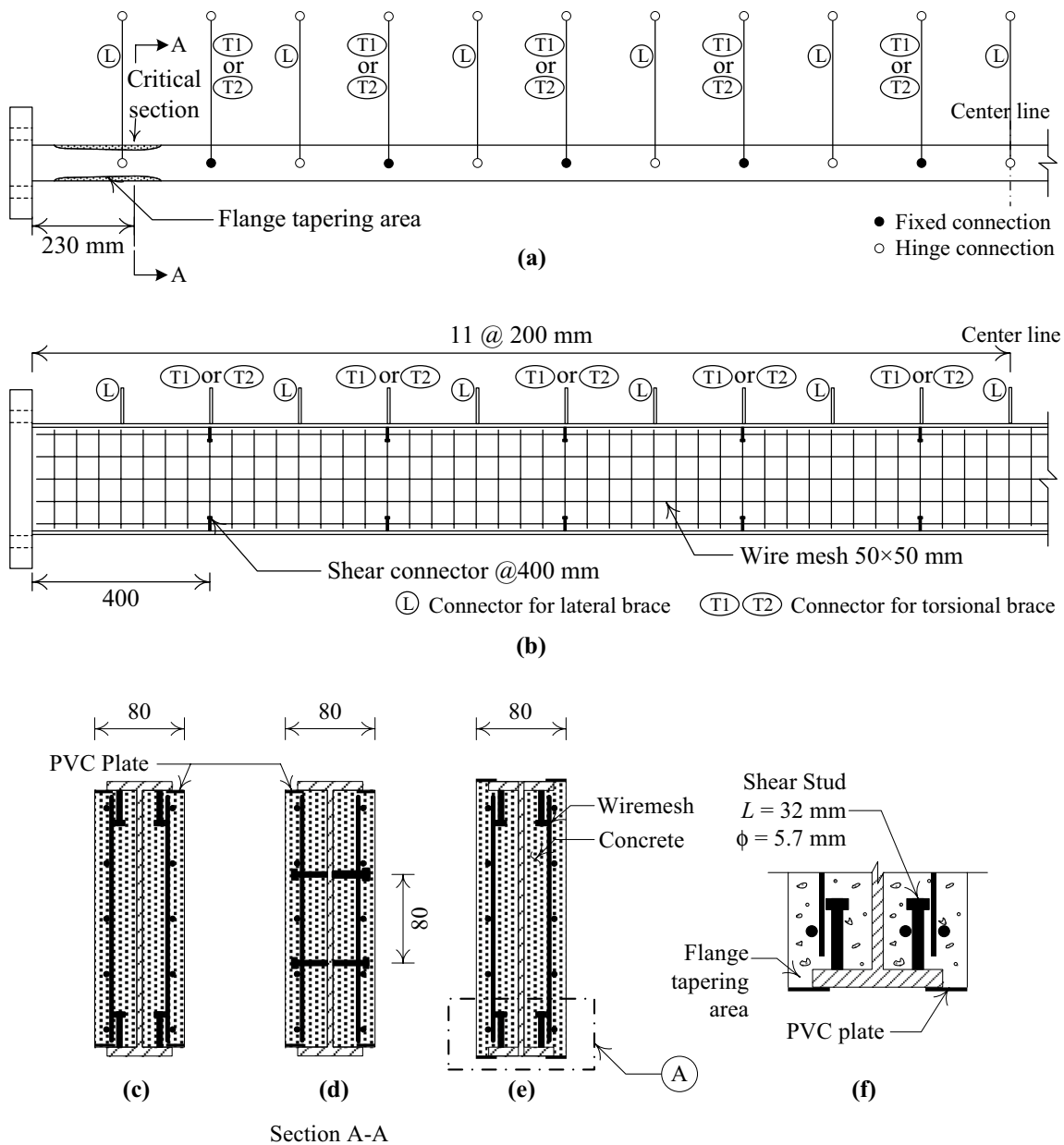
Fig. 7 Detail of specimens in PE series (unit = mm) **a** Top view of test beam, **b** Front view of test beam, **c** PE, **d** PEw, **e** PEb, **f** Detail A

shown in Fig. 11, to measure the lateral displacement Δ_L and Δ_R. Since the largest difference between Δ_L and Δ_R is less than 1%, an average value Δ is used as frame lateral displacement. Quasi-static cyclic load was applied under displacement control with a loading history as shown in Fig. 12. Drift ratio α is defined as ratio of lateral displacement Δ to H_c (shown in Fig. 11). The loading history used in this experiment adopted the loading sequence specified in Section K2.4b ANZI/AISC 341-16.

Two strain gages were attached on each torsional brace, as shown in Fig. 9, to monitor the moment, which is the torsion to the beam, of the torsional brace. Loading test was terminated when one of the following conditions was met: (1) the strength of the specimen deteriorated more than 20%, (2) the drift ratio reached 8% rad or (3) the strain in the torsional brace reached the yield strain. The third condition of loading test termination was intended to protect the torsional braces, so it can be used to completed the all tests.
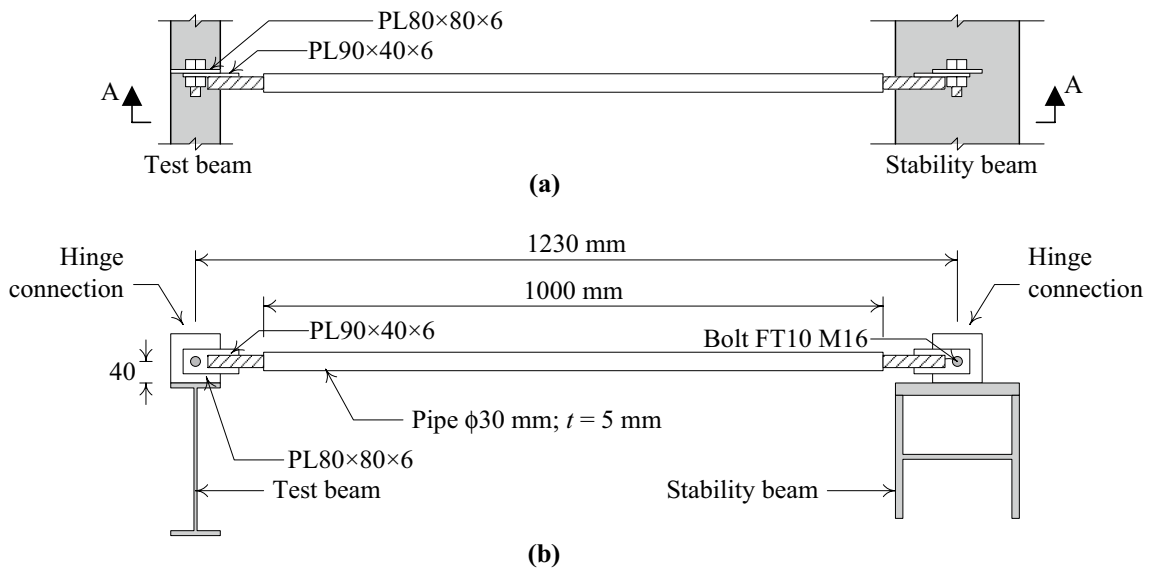
Fig. 8 Detail of lateral brace (unit = mm) **a** Plan view, **b** Section A-A
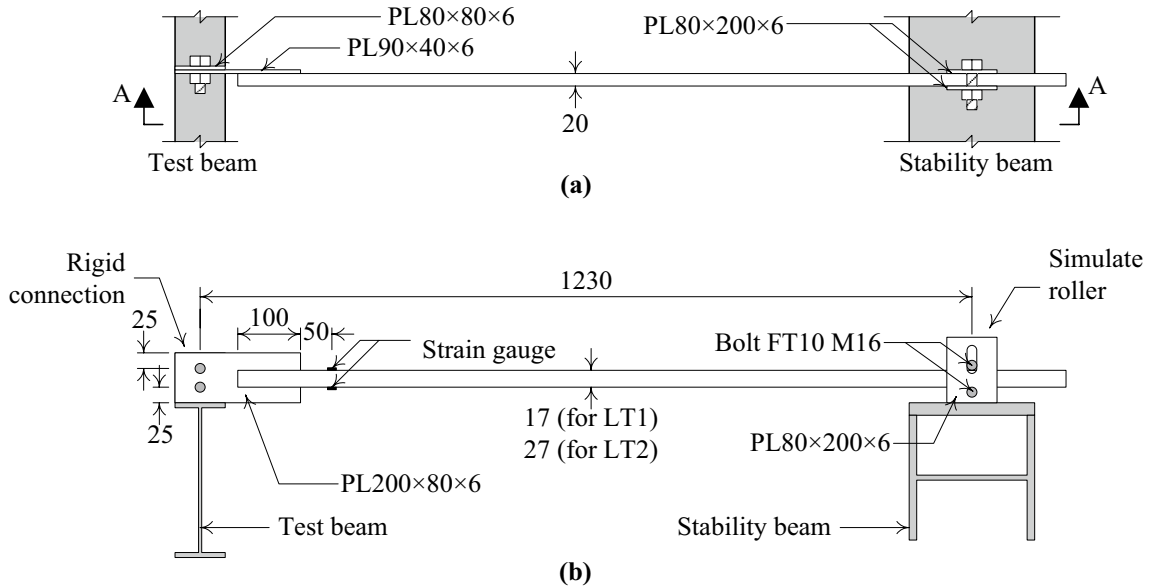
Fig. 9 Detail of torsional brace (unit = mm) **a** Plan view, **b** Section A-A

Table 2 Mechanical properties of steel materials

Item	Yield stress (MPa)	Ultimate stress (MPa)
Beam flange	337	452
Beam web	469	544

3 Experimental Results and Discussion

3.1 General Behavior

The load versus displacement hysteresis loops for all specimens are shown in Fig. 13, and the skeleton curves based on first cycle of each drift ratio excursion are shown in Fig. 14.

Fig. 10 Test setup in 3D view

1. Test beam
2. Column of frame S
3. Actuator
4. Load transfer beam
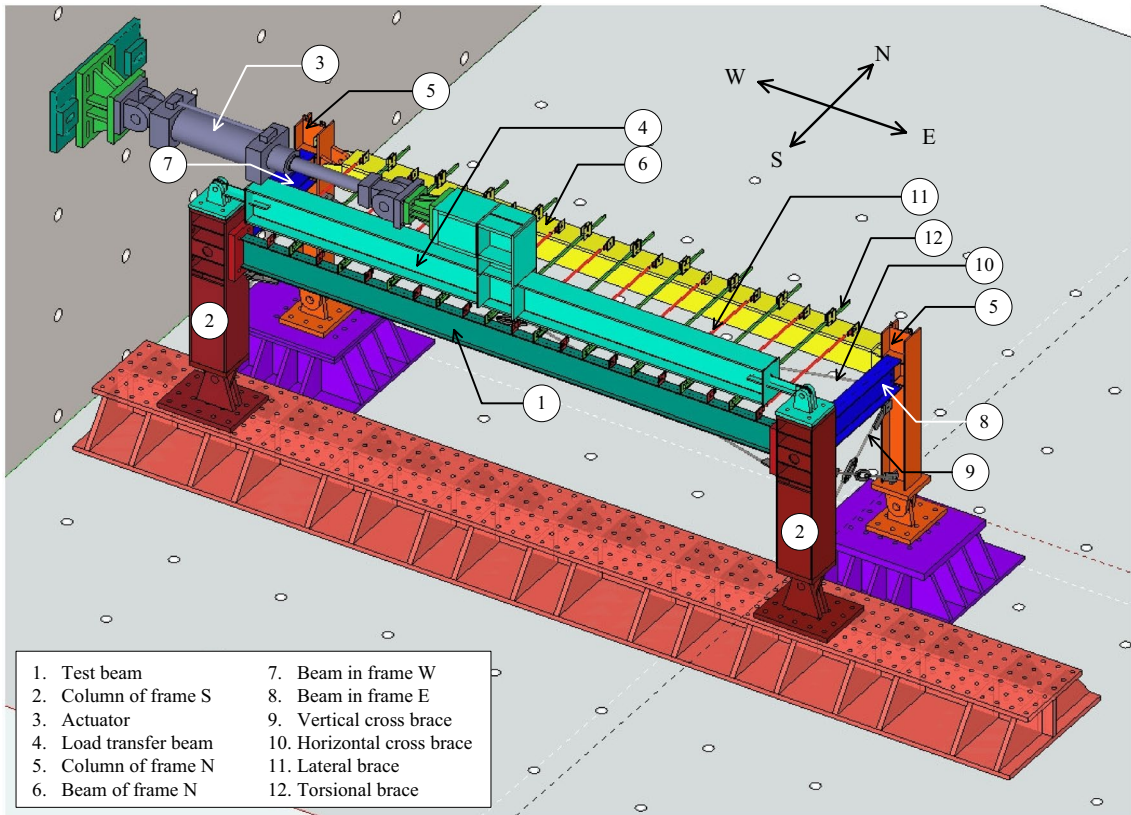5. Column of frame N
6. Beam of frame N
7. Beam in frame W
8. Beam in frame E
9. Vertical cross brace
10. Horizontal cross brace
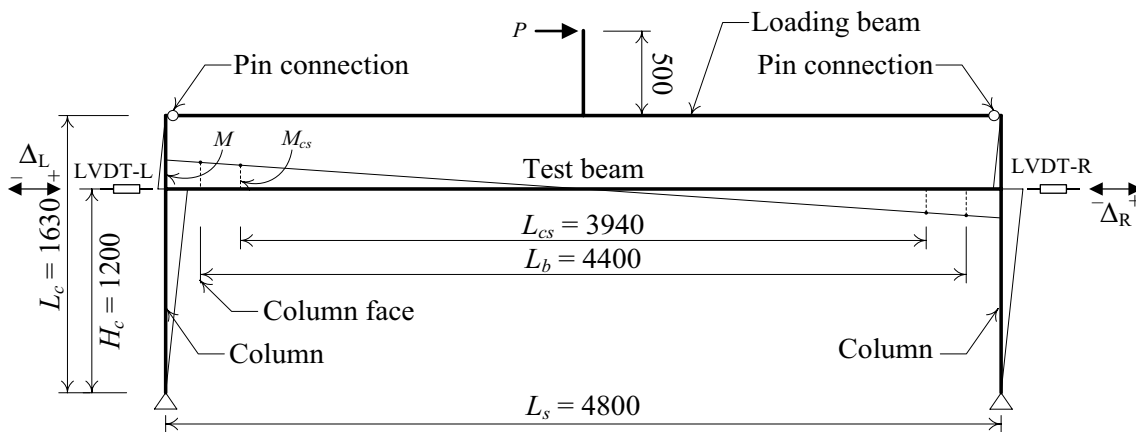11. Lateral brace
12. Torsional brace

Fig. 11 Moment distribution in test beam and column (unit = mm)

The maximum loads in positive and negative directions are designated respectively as P^+_{peak} and P^-_{peak}, and their corresponding drift ratios are designated as α^+_{peak} and α^-_{peak}. The ultimate load for the test specimen P_{exp} is defined as the average of P^+_{peak} and P^-_{peak}. The α_{peak} is defined as the average value of α^+_{peak} and α^-_{peak}. By assuming an anti-symmetric moment distribution as shown in Fig. 11, moment at critical section M_{exp} corresponding to P_{exp} can be calculated and is listed in Table 3. Assuming columns are rigid, the rotations at both beam ends, designated as θ, are identical, and θ is then equal to the applied drift ratio α. The beam end rotation

Fig. 12 Loading history
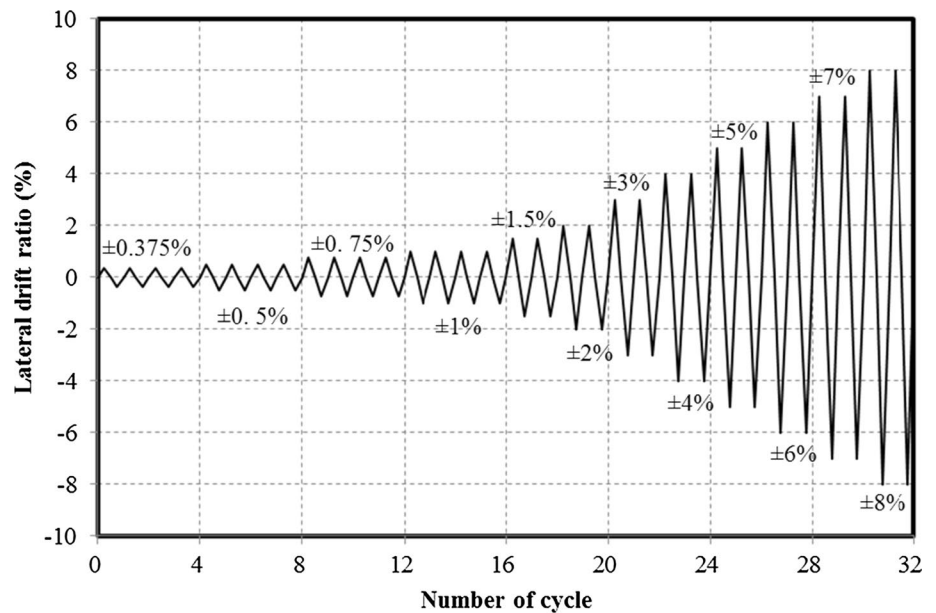
is designated as θ^+ and θ^- as loading applied in positive and negative direction, respectively.

The yield rotation θ_y and ultimate rotation θ_u were determined based on P vs. θ skeleton curve of each specimen. As illustrated in Fig. 15, the elastic stiffness K_e is the initial slope of $P - \theta$ skeleton curve, and θ_y is set equal to P_{peak} divided by K_e. The ultimate rotation θ_u is defined as the θ corresponding to 80% of P_{peak} after P_{peak} is reached. If the strength of the specimen didn't degrade to 80% of P_{peak} at the end of the loading test, the θ_u was assigned as the maximum drift ratio reached during the test. In this case, the real ultimate rotation should be greater than θ_u. Plastic rotation θ_p is defined as the difference between ultimate rotation θ_u and yield rotation θ_y. The θ_y, θ_u and θ_p for all PE specimens are summarized in Table 4.

The ductility also can be evaluated by an indicator named ductility index μ, and it is defined as θ_u divided by θ_p. The ductility index μ of the test specimens are listed in Table 4.

The moment capacity M_{na} of pure steel and PE beams at critical section, as shown in Figs. 7a, c–e and 16a, can be determined based on the measured material yield stress and compressive strength, complete composite action, and plastic stress distribution (Section I1. 2a ANZI/AISC 360-16) as shown on Fig. 16b. The M_{na} for H and PE beams are 69.1 and 75.8 kN-m respectively. The strength ratio γ is defined as the ratio of M_{exp} to M_{na} and is listed in Table 3.

Buckling deformation of H-0 was first observed at drift ratio of 1% rad. The strength of the beam increased very slowly in the following load cycles, however, significant LTB deformation was observed as the drift ratio increased. Figure 17 shows the dramatic LTB deformation of H-0 at drift ratio of $+5\%$ rad. Peak loads occurred at drift ratio of

$\pm 8\%$ rad and there was no strength degradation observed before loading test was terminated. The γ value of H-0 was 0.91, which is less than 1.0. This indicates that the plastic strength of steel section was not fully developed due to significant LTB. Therefore, the ductility of H-0 is not counted and is not discussed in the following sections.

For all the PE specimens, flexural cracks were first observed at drift ratio of 0.5% rad. The cracks continued to develop until peak load, which always occurred at the first cycle of a certain drift ratio, was reached. In the second load cycle of the same drift ratio, strength degradation occurred and concrete on compression side started to crush. And, in the following cycle, concrete spalling was observed and lateral and torsional deformation of the beam become noticeable. Figure 18 shows the concrete damage at end of first cycle of drift ratio of 5% rad. Compared to H-0, lateral and torsional deformation of PE specimens occurred at much larger drift ratio and was much less severe. For specimens with torsional braces, the test was stopped when the maximum strain in torsional braces approaching yield strain, and the strength of the specimen have not deteriorated more than 20%. Therefore, the θ_u and μ of specimens PE-LT1, PE-LT2, PEb-LT2, and PEw-LT2 should be greater than the experimental values as listed in Table 4.

The γ values of all PE specimens range from 1.03 to 1.15 and are larger than 1.0. This indicates that event PE specimens have developed their plastic moment capacity. Except for PE-0, all specimens in the PE series can achieve plastic rotation larger than 4% rad, which satisfies the requirement for a highly ductile member in seismic design as stated in AISC seismic provision (2016).
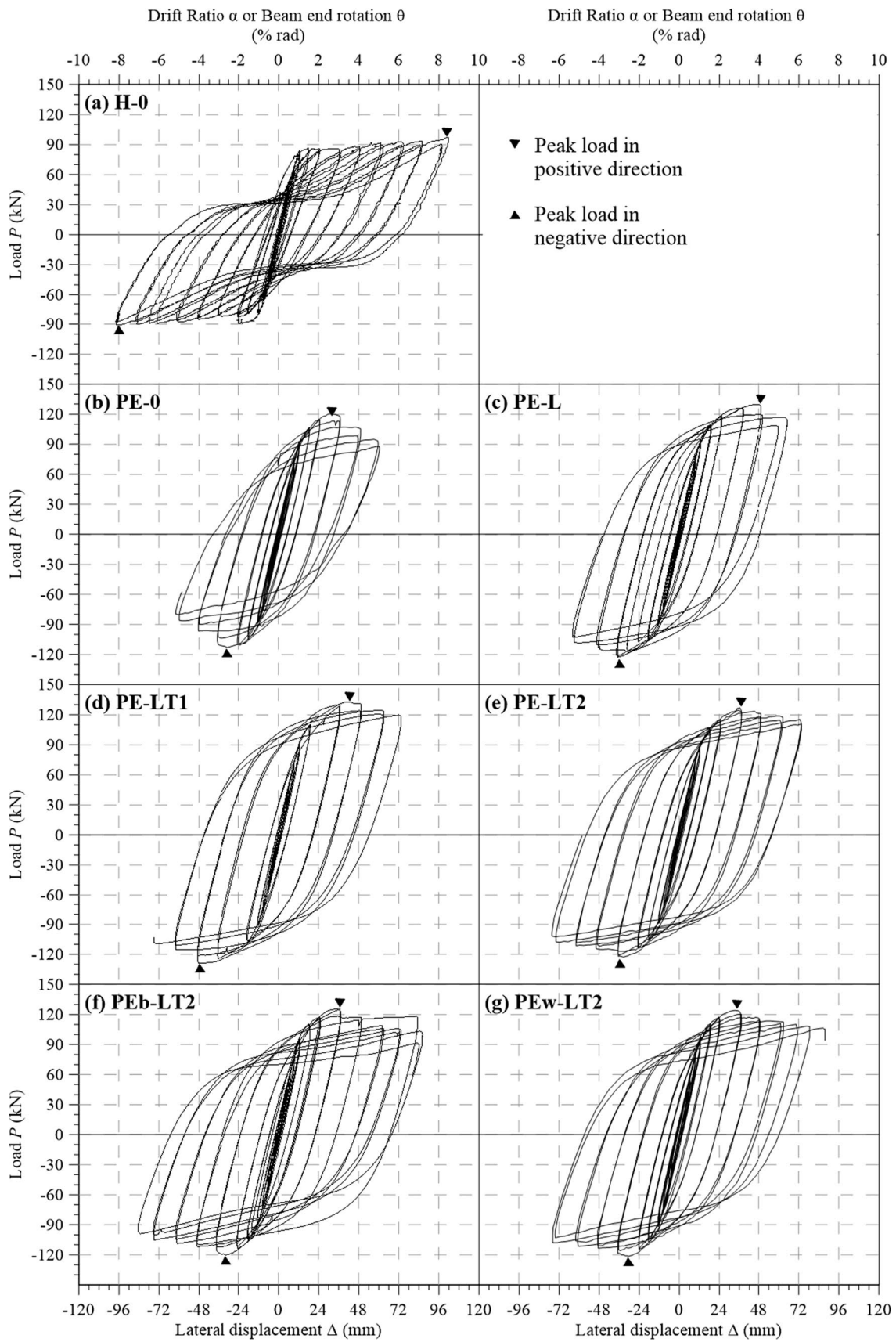
Fig. 13 Load versus displacement hysteretic loops

Fig. 14 Skeleton curve for all specimens **a** Specimen H-0, PE-0, PE-L, PE-LT1 and PE-LT2. **b** Specimen PE-LT2, PEb-LT2 and PEw-LT2
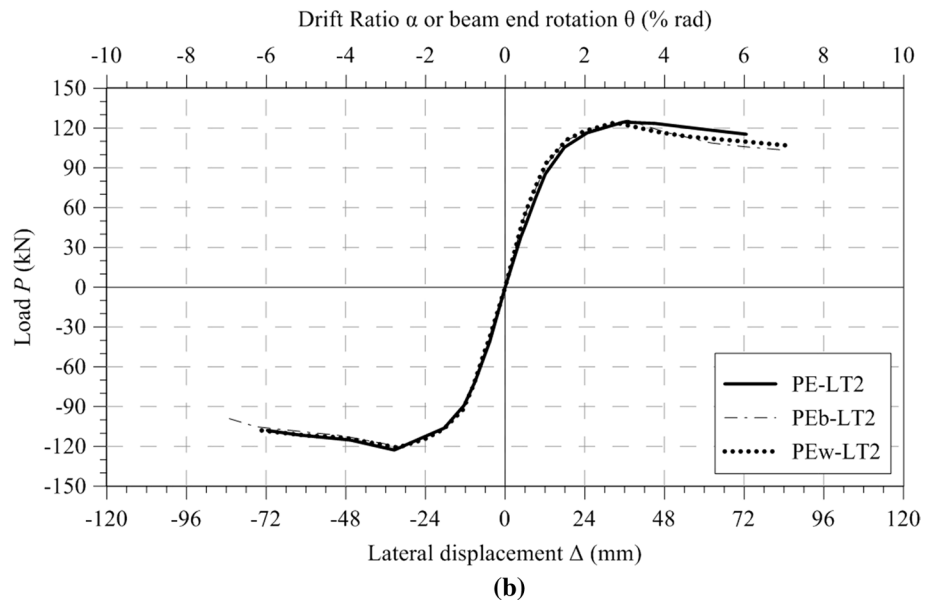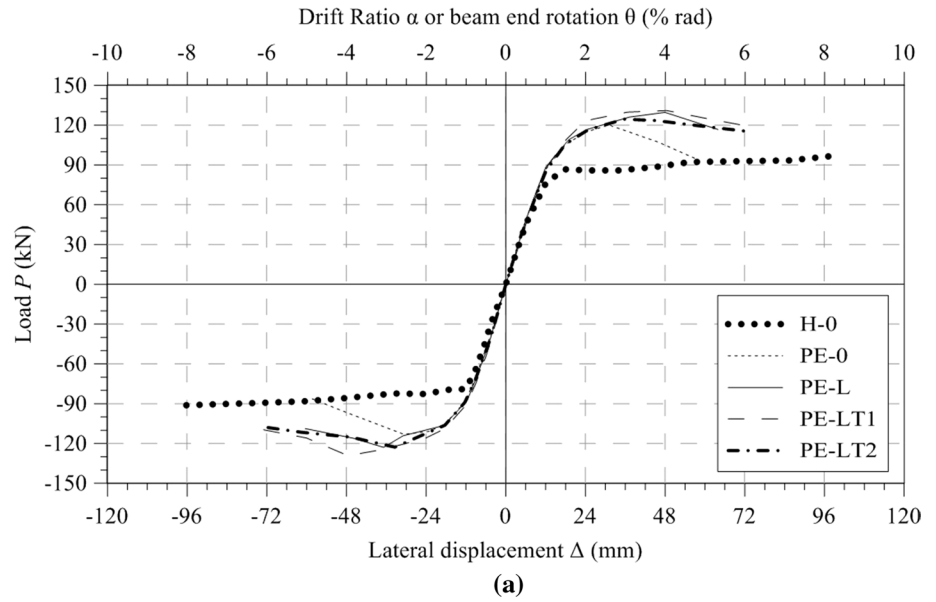

(a)

(b)

Table 3 Test results

Series	Specimen	P^+_{peak} (kN)	α^+_{peak} (% rad)	P^-_{peak} (kN)	α^-_{peak} (% rad)	P_{exp} (kN)	α_{peak} (% rad)	M_{exp} (kN-m)	γ
H	H-0	97	8.0	91	8.0	94	8.00	63.0	0.91
PE	PE-0	120	2.5	113	2.5	117	2.50	78.0	1.03
	PE-L	130	4.0	123	3.0	126	3.50	84.5	1.11
	PE-LT1	131	3.5	129	4.0	130	3.75	87.0	1.15
	PE-LT2	125	3.0	123	3.0	124	3.00	82.7	1.09
	PEb-LT2	126	3.0	120	2.5	123	2.75	82.4	1.09
	PEw-LT2	124	3.0	121	2.5	123	2.75	82.0	1.08
Average for PE series						125			1.09

Fig. 15 Definition of θ_y, θ_u and θ_p

Fig. 16 Critical section and plastic stress distribution of PE beam **a** Critical section. **b** Plastic stress distribution
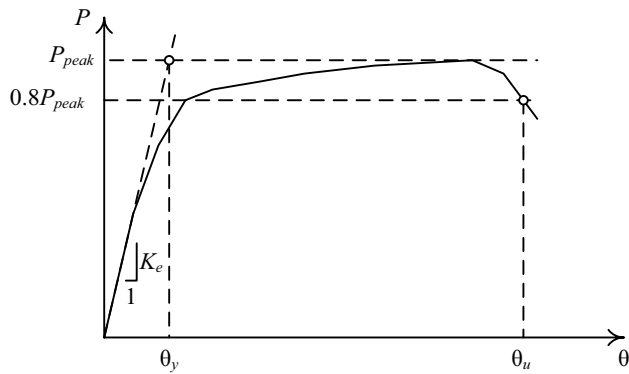
3.2 The Effect of Concrete Encasement

The nominal flexural strength of the PE section, considering full composite action, is 9.6% higher than the H section. Test results show that the γ of PE-0 (1.03) is greater than 1.0, which indicates that composite action in PE-0 was fully developed and the concrete encasement was able to prevent the beam from LTB before concrete was crushed.

After peak load was reached, the strength degraded rapidly. This rapid strength degradation limited the plastic rotation capacity that could be achieved by PE-0. Although the ultimate rotation capacity of PE-0 reached 4.6% rad, the plastic rotation capacity of PE-0 is 3.42% rad which is slightly less than 4% rad and is considered inadequate for seismic design of highly ductile members as required by AISC seismic provision (2016). The ductility index of PE-0 is 3.92 which is slightly less than 4.0, indicating that this specimen is not quite satisfy ductility requirement for structure under seismic loading.

Although concrete encasement can raise the moment capacity of the beam and ensure the PE beam reaches its plastic moment before instability occurs, a bare PE beam without any lateral support is still insufficient to satisfy the requirement for highly ductile flexural members.
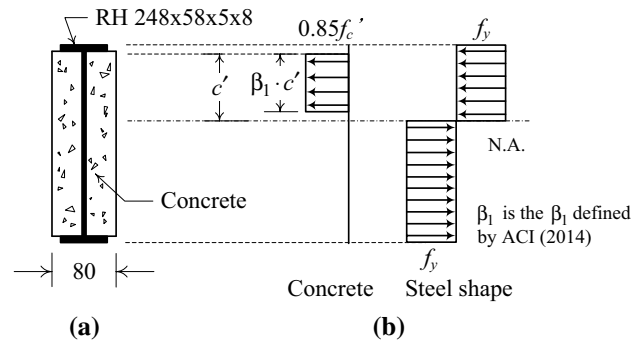
3.3 The Effect of Lateral and Torsional Support

The performance of PE-L is superior to PE-0 in many ways, which is mainly due to the effect of the lateral support. The γ value of PE-L is 1.11 which is obviously higher than 1.03 for PE-0, in addition, the θ_{peak} of PE-L (3.5% rad) is higher than PE-0 (2.5% rad). These indicate that lateral support makes the beam more stable and enables the beam to develop its strength more completely.

The θ_u and θ_p of PE-L are, respectively, at least 13 and 15% higher than those of PE-0. And the ductility index of PE-L is 4.14, which is about 5% higher than PE-0. The seismic performance of PE-0 is barely enough for highly ductile members. However, with the existence of the lateral support at top flange, the performance of the member is elevated and basically fulfills the requirements for highly ductile members.

As indicated in Tables 3 and 4, the γ value of PE-LT1 and PE-LT2 are similar to that of PE-L, however, the ductility, in terms of θ_u and θ_p, of PE-LT1 and PE-LT2 is higher than PE-L. The existence of torsional braces was able to add extra ductility to the beam.

Table 4 Plastic rotation capacity and ductility index	Specimen	θ_y^+ (% rad)	θ_y^- (% rad)	θ_u^+ (% rad)	θ_u^- (% rad)	θ_y (% rad)	θ_u (% rad)	θ_p (% rad)	μ
	PE-0	1.21	1.13	4.66	4.51	1.17	4.59	3.42	3.92
	PE-L	1.35	1.16	5.33	5.04	1.26	5.19	3.93	4.14
	PE-LT1	1.48	1.14	> 6.02	> 6.08	1.30	> 6.05	> 4.75	> 4.65
	PE-LT2	1.29	1.16	> 6.05	> 5.97	1.23	> 6.01	> 4.79	> 4.91
	PEb-LT2	1.10	1.28	> 7.05	> 6.93	1.19	> 6.99	> 5.81	> 5.87
	PEw-LT2	1.06	1.25	> 7.22	> 6.11	1.16	> 6.67	> 5.51	> 5.77

Fig. 17 Lateral torsional buckling (LTB) at drift ratio of 5% rad
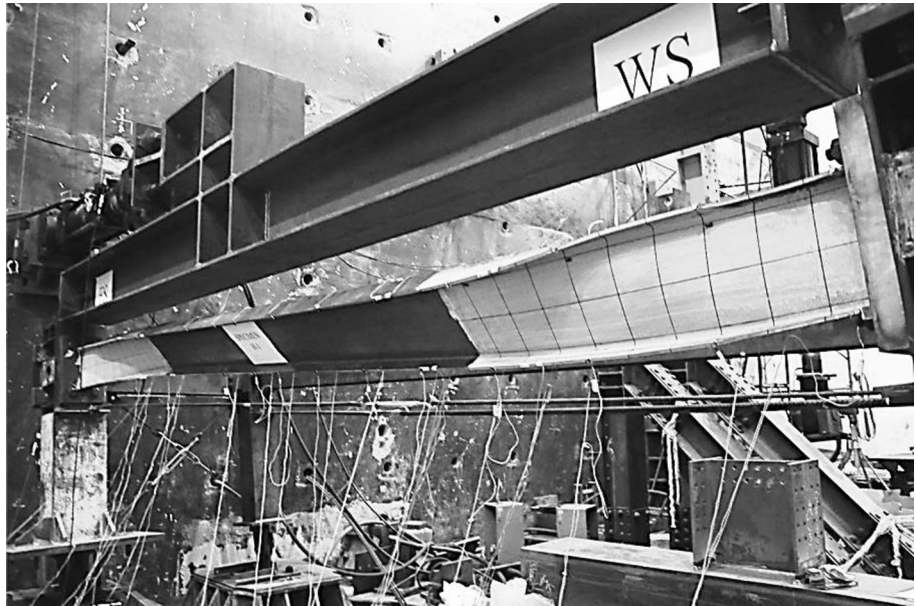
3.4 The Effect of Structural Details

The performance of specimen PEb-LT2, which had concrete in the flange tapering area, is slightly worse than PE-LT2. On the compression side of the beam, the flange imposes compressive force on the flange concrete, at the same time, an out-of-plane force component pushed the flange concrete sideward, as shown in Fig. 19, and damaged the concrete. Therefore, it is recommended not to fill concrete into the flange tapering area.

The performance of specimen PEw-LT2, which had shear connectors welded on the web plate, is about the same as PE-LT2. Therefore, the location of shear connectors has limited effect to the behavior of PE beam as long as the number of shear connectors used is the same.

4 Conclusion

Seven reduced scale full span beam specimens, consisting of one bare steel beam and six partially concrete encased steel beams (PE beam), were fabricated and tested under cyclic loading to investigate the hysteretic behavior of PE beams. Based on the experimental results reported herein, the following conclusions can be drawn:

1. Due to lateral torsional buckling, the bare steel beam showed the following behaviors: strength development was insufficient, the pinching of hysteresis loops was obvious, and the lateral and torsion deformation were significant.
2. When stood alone, a PE beam was able to develop its plastic strength and a plastic rotation capacity of 3.42% rad. The concrete on PE beam showed significant effect in providing stability capacity to the steel beam.
3. When lateral brace on top flange was provided, PE beam not only could develop its plastic strength but also possess a plastic rotation capacity higher than 3.93% rad and with ductility index of 4.14. This means as soon as a PE beam is connected to a slab, disregarding the possible torsional bracing effect that the slab can provide, the PE beam is able to develop enough strength and ductility for structures in high seismic zones. If the torsional bracing effect of the slab is considered, the plastic rotation capacity of PE beam can be elevated to 4.79% rad and possesses the ductility index higher than 4.91.
4. The placement of shear studs, either on flange or on web, does not affect either strength or ductility development of PE steel beam.
5. The presence of concrete in the area where the beam flange was tapered may have caused minor local concrete damage and the presence of concrete in this area
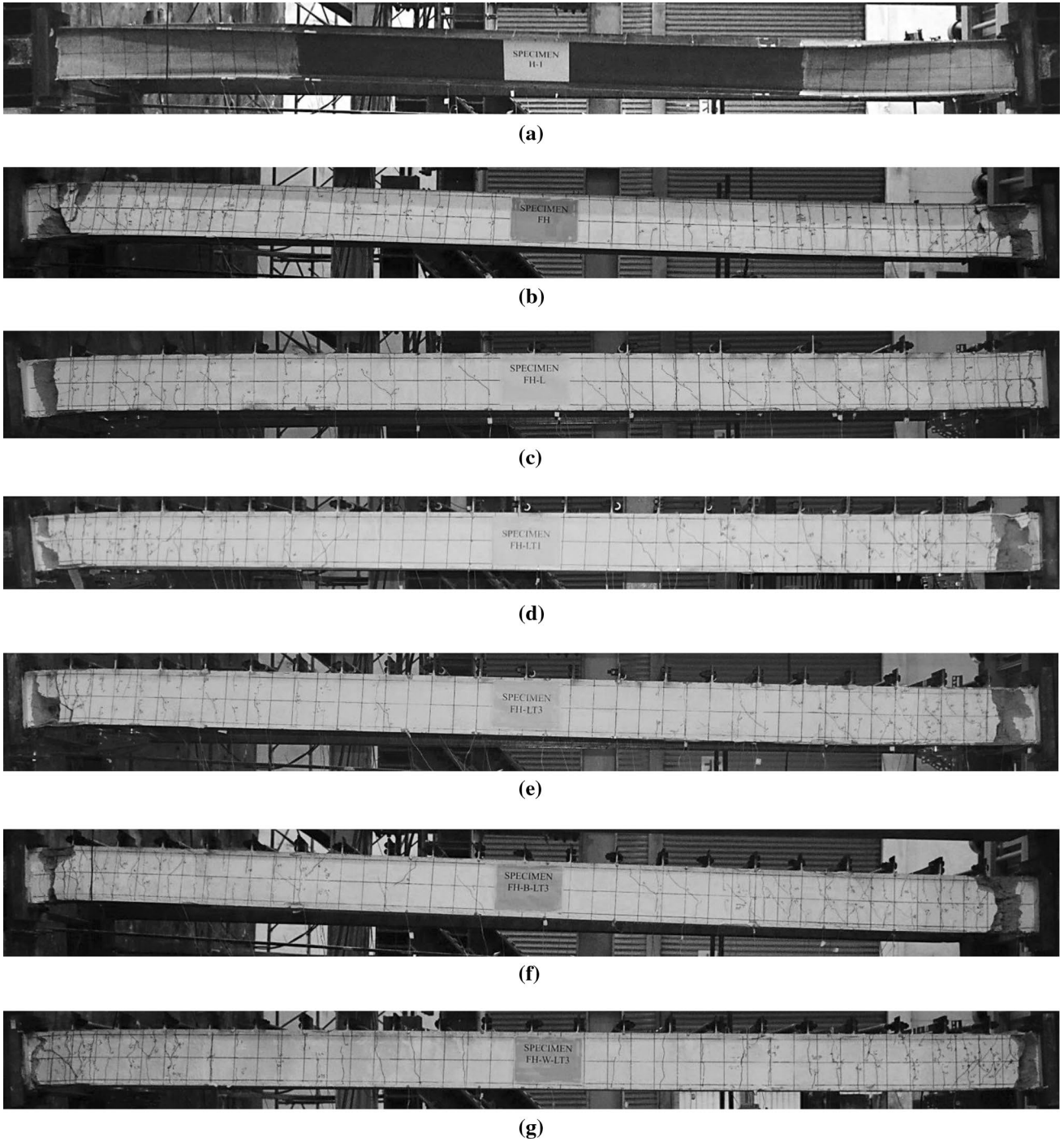
(a)

(b)

(c)

(d)

(e)

(f)

(g)

Fig. 18 Appearance of all specimens at drift ratio of 5% rad **a** Specimen H-0, **b** Specimen PE-0, **c** Specimen PE-L, **d** Specimen PE-LT1, **e** Specimen PE-LT2, **f** Specimen PEb-LT2, **g** Specimen PEw-LT2
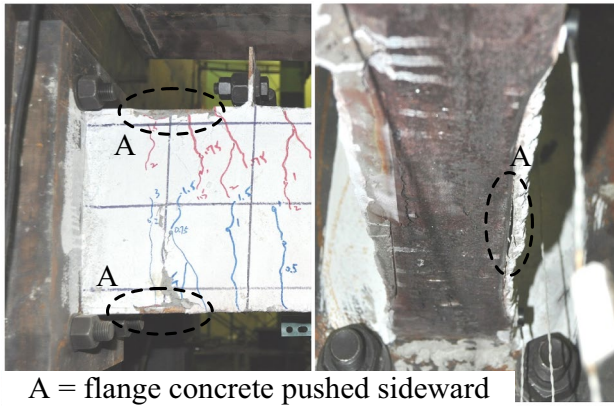
A = flange concrete pushed sideward

Fig. 19 Concrete crush earlier (drift ratio of 3% rad) in PEb-LT2

had insignificant negative effect on the performance of PE steel beam.

References

ACI. (2014). *Building code requirement for structural concrete ACI 318-99* . Farmington Hills: American Concrete Institute.

ANSI, AISC 341-16. (2016). *Seismic provision for structural steel buildings*. Chicago: American Institute of Steel Construction.

ANSI, AISC 360–16. (2016). *Specification for structural steel buildings*. Chicago: American Institute of Steel Construction.

Chen, S. J. (2001). Design of ductile seismic moment connection, increased beam section method and reduced beam section method. *International Journal of Steel Structures, 1,* 45–52.

Chen, S. J., Yeh, C. H., & Chu, J. M. (1996). Ductile steel beam-to-column connection for seismic resistance. *Journal of Structural Engineering, ASCE, 122*(11), 95–119.

Chen, Y., Li, W., & Fang, C. (2017). Performance of partially encased composite beams under static and cyclic bending. *Structures, 9,* 29–40.

De Nardin, S., & El Debs, A. L. H. (2009). Study of partially encased composite beams with innovative position of stud bolts. *Journal of Constructional Steel Research, 65*(2), 342–350.

Hegger J., & Goralski C. (2005). Structural behavior of partially concrete encased composite sections with high strength concrete. In *Proceedings of the 5th international conference in composite construction in steel and concrete* (pp. 346–355), South Africa.

Itani, A. M., Cheng, Z., & Saiidi, M. (2004). Cyclic response of steel moment connection for large beam sections using haunch and reduced beam section concepts. *International Journal of Steel Structures, 4,* 147–155.

Jiang, Y., Hu, X., Hong, W., Gu, M., & Sun, W. (2017). Investigation on partially concrete encased composite beams under hogging moment. *Advances in Structural Engineering, 20*(3), 461–470.

Jin, J., & El-Tawil, S. (2005). Seismic performance of steel frames with reduced beam section connections. *Journal of Constructional Steel Research, 61,* 453–471.

Kindmann, R., Bergmann, R., Cajot, L.-G., & Scleich, J. B. (1993). Effect of reinforced concrete between the flanges of the steel profile of partially encased composite beams. *Journal of Constructional Steel Research, 27*(1–3), 107–122.

Kodaira, A., Fujinaka, H., Ohashi, H., & Nishimura, T. (2004). Fire resistance of composite beams composed of rolled steel profile concreted between flanges. *Fire Science and Technology, 23*(3), 192–208.

Lindner J. & Budassis N. (2000). Lateral torsional buckling of partially encased composite beams without concrete slab. In *Proceedings of composite construction in steel and concrete IV conference*, The United Engineering Foundation ASCE (pp. 117–128), Canada.

Nakamura, S., & Narita, N. (2003). Bending and shear strengths of partially encased composite I-girders. *Journal of Constructional Steel Research, 59,* 1435–1453.

Piloto P. A. G., Gavilan A. B. R., Mesquita L. M. R., & Goncalves C. (2012). High temperature tests on partially encased beams. In *Proceedings of the 7th international conference on structures in fire*, Zurich, Switzerland.

Piloto, P. A. G., Gavilan, A. B. R., Zipponi, M., Marini, A., Mesquita, L. M. R., & Plizzari, G. (2013). Experimental investigation of the fire resistance of partially encased beams. *Journal of Constructional Steel Research, 80,* 121–137.

Plumier, A. (1994). Behavior of connections. *Journal of Constructional Steel Research, 29,* 95–119.